

The HARPS search for southern extra-solar planets. XXXV. Super-Earths around the M-dwarf neighbors Gl 433 and Gl 667C [★]

X. Delfosse¹, X. Bonfils¹, T. Forveille¹, S. Udry², M. Mayor², F. Bouchy³, M. Gillon⁴, C. Lovis², V. Neves^{1,5,6}, F. Pepe², C. Perrier¹, D. Queloz², N.C. Santos^{5,6}, and D. Ségransan²

¹ UJF-Grenoble 1 / CNRS-INSU, Institut de Planétologie et d'Astrophysique de Grenoble (IPAG) UMR 5274, Grenoble, F-38041, France

² Observatoire de Genève, Université de Genève, 51 ch. des Maillettes, 1290 Sauverny, Switzerland

³ Institut d'Astrophysique de Paris, CNRS, Université Pierre et Marie Curie, 98bis Bd. Arago, 75014 Paris, France

⁴ Université de Liège, Allée du 6 août 17, Sart Tilman, Liège 1, Belgium

⁵ Centro de Astrofísica, Universidade do Porto, Rua das Estrelas, 4150-762 Porto, Portugal

⁶ Departamento de Física e Astronomia, Faculdade de Ciências, Universidade do Porto, Rua do Campo Alegre, 4169-007 Porto, Portugal

Received / Accepted

ABSTRACT

Context. M dwarfs have been found to often have super-Earth planets with short orbital periods. Such stars are thus preferential targets in searches for rocky or ocean planets in the solar neighbourhood.

Aims. In a recent paper (Bonfils et al. 2011), we announced the discovery of respectively 1 and 2 low mass planets around the M1.5V stars Gl 433 and Gl 667C. We found those planets with the HARPS spectrograph on the ESO 3.6-m telescope at La Silla Observatory, from observations obtained during the Guaranteed Time Observing program of that instrument.

Methods. We have obtained additional HARPS observations of those two stars, for a total of respectively 67 and 179 Radial Velocity measurements for Gl 433 and Gl 667C, and present here an orbital analysis of those extended data sets and our main conclusion about both planetary systems.

Results. One of the three planets, Gl 667Cc, has a mass of only $M_2 \cdot \sin i \sim 4.25 M_{\oplus}$ and orbits in the central habitable zone of its host star. It receives just 10% less stellar energy from Gl 667C than the Earth receives from the Sun. However planet evolution in habitable zone can be very different if the host star is a M dwarf or a solar-like star, without necessarily questioning the presence of water. The two other planets, Gl 433b and Gl 667Cb, both have $M_2 \cdot \sin i$ of $\sim 5.5 M_{\oplus}$ and periods of ~ 7 days. The Radial Velocity measurements of both stars contain longer time scale signals, which we fit as longer period Keplerians. For Gl 433 that signal probably originates in a Magnetic Cycle, while a longer time span will be needed to conclude for Gl 667C. The metallicity of Gl 433 is close to solar, while Gl 667C is metal poor with $[\text{Fe}/\text{H}] \sim -0.6$. This reinforces the recent conclusion that the occurrence of Super-Earth planets does not strongly correlate with stellar metallicity.

Key words. techniques : radial velocity / stars : late-type / planetary systems

1. Introduction

Much interest has recently focused on planets around M dwarfs, with three main motivations: constraining formation, physico-chemical characterization of planets, and finding rocky planets in the habitable zone of their stars. The compared occurrence frequency, as a function of orbital elements, of planets around M dwarfs and around the more massive solar-type stars probes the sensitivity of planetary formation to its initial conditions. Giant planets are rare around M dwarfs, with Bonfils et al. (2011a), for instance, finding a low frequency of $6_{-2}^{+6}\%$ for periods under 10000 days. That number is lower than the $10 \pm 2\%$ frequency for similar planets around solar-like stars (e.g. Mayor et al. 2011), though not yet at a high significance level. Super-Earth (2-10 M_{\oplus}), by contrast, seem abundant around M dwarfs at the short orbital periods to which radial velocity searches are most sensitive: Bonfils et al. (2011a) find an occurrence rate of $88_{-19}^{+55}\%$ for

$P < 10$ days, to be compared to $\sim 50\%$ for similar planets around G dwarfs.

The physical conditions in the circumstellar disks of very low mass stars therefore favor the formation of low-mass planets (rocky and maybe ocean planets) close to the star. This translates into good odds for finding telluric planets transiting M dwarfs (like those very recently announced by Muirhead et al. 2012). Such transiting planets are excellent atmospheric characterization targets: since transit depth scales with the squared stellar radius, a transit across an M dwarf provides much more accurate measurements of radius and transmission spectrum than across a solar-type star.

Finding rocky planets in the habitable zone (HZ) of their stars is another motivation for planet searches around M dwarfs. Planets of given mass and orbital separation induce larger stellar radial velocity variation around lower mass stars, but, more importantly, the low luminosity of M dwarfs moves their habitable zone much nearer to the star. These two effects combine, and a habitable planet around a 0.3- M_{\odot} M dwarf produces a 7 times larger radial velocity wobble than the same planet orbiting a solar-mass G dwarf. Additionally, some atmospheric

[★] Based on observations collected with HARPS instrument on the 3.6-m telescope at La Silla Observatory (European Southern Observatory) under programs ID072.C-0488(E)

models suggest additional advantages of planets in the HZ of M dwarfs for habitability characterization: Segura et al. (2005) find that the significant dependence of atmospheric photochemistry on the incoming spectral energy distribution strongly reinforces some biomarkers in the spectra of Earth-twin planets orbiting M dwarfs. N_2O and CH_3Cl , in particular, would be detectable for Earth-twin planets around M dwarfs but not around solar-type stars.

As discussed in Bonfils et al. (2011a), which presents the full specifications of the survey, we have been monitoring the radial velocities (RV) of a distance and magnitude limited sample of 102 M dwarfs since 2003 with the HARPS spectrograph mounted on the ESO/3.6-m La Silla telescope. With a typical RV accuracy of 1-3m/s and 460 hours of observations, our survey identified super-Earth and Neptune-like planets around Gl 176 (Forveille et al. 2009), Gl 581 (Bonfils et al. 2005b; Udry et al. 2007; Mayor et al. 2009) and Gl 674 (Bonfils et al. 2007). In Bonfils et al. (2011a), which was centered on the statistical implications of the survey for planet populations, we added to this list 1 planet around Gl 433 and 2 around Gl 667C, providing detailed periodograms and a false alarm probability in using our GTO/HARPS data. Anglada-Escudé et al. (2012) recently announced a confirmation of the planets Gl 667Cb and Gl 667Cc, which however is only very partly independent, since it largely rests on our Bonfils et al. (2011a) observations and data reduction.

Here we present a more detailed orbital analysis of these two systems than we could present in Bonfils et al. (2011a), and we refine their parameters by adding new seasons of RV measurements. The 3 super-Earths have $M_2 \cdot \sin i$ between 4.25 and 5.8 M_\oplus . With periods of ~ 7 days, both Gl433b and Gl667Cb are hot super-Earths. Gl667Cc, by contrast, has a 28-day period. It orbits in the centre of the habitable zone of its star, and receives just 10% less stellar energy than the Earth receives from the Sun. We also detect some longer-period radial-velocity variations, which we also discuss.

The next section discusses our data taking and analysis, while Sect. 3 summarizes the stellar characteristics of Gl 433 and Gl 667C. Sect. 4 and 5 respectively present our orbital analyses of the planetary systems of Gl 433 and Gl 667C. Sect. 6 discusses the habitable zones of M dwarfs, with emphasis on the case of Gl 667Cc. Finally, Sect.7. summarizes our conclusions.

2. Spectroscopic and Doppler measurement with HARPS

Our observing procedure is presented in some details in Bonfils et al. (2011a), and is only summarized here. For both stars we obtained 15 min exposures with the HARPS spectrograph (High Accuracy Radial velocity Planets Searcher Mayor et al. 2003). HARPS is a fixed-format echelle spectrograph, which covers the 380 to 630 nm spectral range with a resolving power of 115 000. HARPS is fed by a pair of fibres, and is optimized for high accuracy radial-velocity measurements, with a stability better than 1m/s during one night. To avoid light pollution on the stellar spectrum of our “faint” M-dwarf targets, we chose to keep dark the calibration fiber of the spectrograph. Our Radial Velocity accuracy is therefore intrinsically limited by the instrumental stability of HARPS. That stability is however excellent and the signal-to-noise ratio of our 15min exposures of these two $V \sim 10$ M dwarfs limits the RV precision to slightly above 1 m/s (the median S/N ratio per pixel at 550nm is 57 and 65 respectively for Gl 433 and Gl 667C). Sect. 4 and 5 discuss the number of exposures and their time span for the two stars.

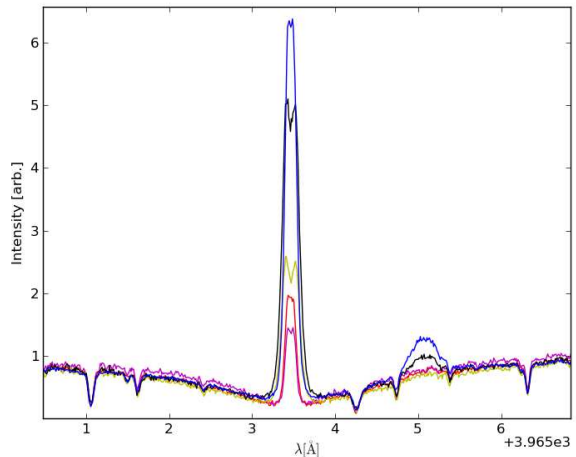


Fig. 1. Emission reversal in the Ca II H line in the average spectra of (from the less to the more active) Gl 581 (M3, in magenta), Gl 667C (M1.5, in pink), Gl 433 (M1.5, in yellow), Gl 176 (M2.5, dark) and Gl 674 (M3, in blue). Within our 100 M dwarfs sample, Gl 581 has one of the weakest Ca II emission and illustrates a very quiet M dwarf. Gl 674 and Gl 176 have a much stronger emission and are both moderately active with an identified rotational period of respectively 35 and 39 days (Bonfils et al. 2007; Forveille et al. 2009).

For homogeneity, we reprocessed all spectra with the latest version of the standard HARPS pipeline. The pipeline (Lovis & Pepe 2007) uses a nightly set of calibration exposures to locate the orders, flat-field the spectra (Tungsten lamp illumination) and to precisely determine the wavelength calibration scale (ThAr lamp exposure). We measured the Radial Velocity through cross correlation of the stellar spectra with a numerical weighted mask, following the procedure of Pepe et al. (2002). For both Gl 433 and Gl667C, we used a mask derived from a very high S/N spectrum of a M2 dwarf. The velocities of Gl 433 and Gl 667C have internal median errors of respectively 1.15 and 1.30 m/s. This includes the uncertainty of the nightly zero point calibration, the drift and jitter of the wavelength scale during a night, and the photon noise (the dominant term here).

Because both stars have significant proper motion, the projection of their velocity vector changes over the duration of our survey. We subtract this secular acceleration (see Kürster et al. 2003, for details) before radial velocity analysis. For Gl 433 and Gl 667C the values are respectively 0.15 and 0.21 m/s/yr.

3. Stellar characteristic of Gl 433 and Gl 667C

Both Gl 433 (LHS 2429) and Gl 667C are early-M dwarfs in the close solar neighborhood. Table 1 summarizes their properties. The masses are computed from the K -band absolute magnitudes using the Delfosse et al. (2000) empirical near-infrared mass-luminosity relation. The bolometric correction of Gl 433, and then its luminosity, is computed from the $I - K$ color using the cubic polynomial of Leggett et al. (2000). Those authors directly determined the luminosity of Gl 667C using a combination of flux calibrated observed spectra and synthetic spectra, and we adopt their value.

	Gl 433	Gl 667C
Spectral type ⁽¹⁾	M1.5	M1.5
V	9.79	10.22
J ⁽²⁾	6.47±0.02	6.85±0.02
H ⁽²⁾	5.86±0.04	6.32±0.04
K ⁽²⁾	5.62±0.02	6.03±0.02
π	110.6±1.8 ⁽³⁾	138.2±0.7 ⁽⁴⁾
M (in M_{\odot}) ⁽⁵⁾	0.48	0.33
L (in L_{\odot}) ⁽⁶⁾	0.034	0.014
[Fe/H] ⁽⁷⁾	-0.22	-0.55
Teff ⁽⁸⁾	3600	3600
log R_X ⁽⁹⁾	<-4.8	<-4.12

Table 1. (1) Hawley et al. (1996); (2) Cutri et al. (2003); (3) Perryman et al. (1997); (4) Söderhjelm (1999); (5) from mass-luminosity relation of Delfosse et al. (2000); (6) Leggett et al. (2000); (7) from luminosity-color relation of Bonfils et al. (2005a); (8) Morales et al. (2008); (9) from Schmitt et al. (1995) for Gl 433 and from Schmitt & Liefke (2004) for Gl 667C

3.1. Gl 433 : metallicity, activity and dynamic population

According to Bonfils et al. (2005a) we estimated the metallicity of Gl 433 to [Fe/H]~-0.2. This photometric calibration relationship is based on a faint number of stars in the high metallicity range but Neves et al. (2012) show that for such value of [Fe/H] the calibration is correct with a typical dispersion of 0.2 dex. This is confirmed by the value of [Fe/H]=-0.13 obtained in using Neves et al. (2012) relationship, itself an update from Schlaufman & Laughlin (2010). We could conclude that Gl 433 is solar or slightly sub-metallic.

Gl 433 is dynamically classified as a membership of old disk (Leggett 1992). Ca II H and K chromospheric emission is determined by Rauscher & Marcy (2006) and Gl 433 is in the less active half of M dwarfs with same luminosity. For objects of similar spectral type a direct comparison of Ca II emission lines gives relative estimation of rotational period (larger Ca II emissions correspond to shorter rotational periods). In the Fig 1 we present an average HARPS spectrum of Gl 433 in the region of Ca II H line. Gl 433 has an emission of Ca II slightly higher than Gl 581 (a very quite M dwarf), but well below those of Gl 176 and Gl 674 for whose rotational periods of respectively 35 and 39 days have been determined by Bonfils et al. (2007) and Forveille et al. (2009). The five M dwarfs of the Fig. 1 do not have identical spectral (from M1.5 to M3) therefore estimation of rotation from the Ca II emission is only indicative. It shows that Gl 433 rotates most probably with a period longer than Gl 176 and Gl 674.

The X-ray flux of Gl 433 is not detected by ROSAT and we use a ROSAT limiting sensitivity of $2.5^{27} \cdot [d/10pc]^2$ erg/s (Schmitt et al. 1995) to estimate $R_X = \text{Log}L_X/L_{BOL} < -4.8$. For an M dwarfs of $\sim 0.5M_{\odot}$ the R_X versus rotation period relation of Kiraga & Stepien (2007) give $P_{rot} > 40$ days for such level of X flux. This inferior limit on the rotation period is coherent with the estimate from the Ca II emission.

3.2. Gl 667C : multiplicity, metallicity, activity and dynamic population

Gl 667C is the lightest and isolated component of a hierarchical triple system, the two others components are a closest couple of K dwarfs. Gl 667AB has a semi-major axis of 1.82 A.U. (period of 42.15 years) and a total mass dynamically determined of $1.27M_{\odot}$ (Söderhjelm 1999). Gl 667C is at a projected dis-

tance of 32.4" of Gl 667AB, giving an expected semi-major axis of ~ 300 A.U. (for a distance of 7.23 pc and a factor of 1.26 between expected and projected semi-major axis, Fischer & Marcy 1992).

The Bonfils et al. (2005a) photometric relationship for Gl667C gives us an estimate of the metallicity of 0.55 dex, which agrees quite well with the spectroscopic determination of [Fe/H]~-0.6 for the primary (Perrin et al. 1988; Zakhohaj & Shaparenko 1996). This demonstrates that the Bonfils et al. (2005a) photometric calibration gives excellent results for low-metallicity M dwarfs. The Neves et al. (2012) relationship gives [Fe/H]~-0.45, confirming that this star is a metal-poor M dwarfs.

Consistent with this chemical composition, Gl667 is classified as member of the old disk population from its UVW velocity (Leggett 1992) and is among the objects of lower chromospheric emission for its luminosity (Rauscher & Marcy 2006). In the Fig. 1 the Ca II H line emission of Gl 667C is slightly inferior to the Gl 433 one, also indicating also a large rotational period.

The NEXXUS database (Schmitt & Liefke 2004) indicates detection of the X-ray emission of Gl 667C from the ROSAT All-Sky Survey (RASS) with a value of $\text{log} L_X = 27.89$. But the resolution of ROSAT image is not sufficient to separate the three components of the system. Although this value is the jointed flux for Gl 667ABC, it gives a superior limit on the coronal emission of Gl 667C. This implies $R_X = \text{Log}L_X/L_{BOL}$ well below -4.12 and rotational period superior to 40 days (in applying the Kiraga & Stepien (2007) R_X versus rotation period relationship).

4. Orbital analysis of Gl 433

4.1. HARPS measurements

We obtained 67 measurements of Gl433 radial velocity that span 2904 days from December 2003 to November 2011. The data add 17 new points to those analyzed in Bonfils et al. (2011a) and extend their time span by 1200 days. We estimate that the uncertainties of ~ 1.1 m/s are dominated by photon noise (the median S/N ratio per pixel at 550 nm is 57). Overall, the RVs have a rms=3.14 m/s and $\sqrt{\chi^2} = 7.7 \pm 0.5$ per degree of freedom, confirming variability in excess to measurement uncertainties (~ 1.1 m/s, dominated by photon noise).

We therefore continued with a classical periodicity analysis, based on floating-mean periodograms (Gilliland & Baliunas 1987; Zechmeister et al. 2009). Fig. 2 (bottom panel) depicts the periodogram of our RV time series and shows a strong power excess around the period 7.3 day. We plot the window function in Fig. 2 (middle panel) to identify the typical time sampling but found no counter part to this periodicity. We adopted the normalization of periodograms proposed by Zechmeister et al. (2009), which is such that a power of 1 means that a sine function is a perfect fit to the data, whereas a power of 0 indicates no improvement over a constant model. Hence, the most powerful peak was measured at a period $P \sim 7.3$ days with a power $p_{max} = 0.51$. To assess its fortuity we performed a bootstrap randomization (Press et al. 1992): we generated 10,000 virtual data sets by shuffling the actual radial velocities and retaining the dates; for each set we computed a periodogram; with all periodograms we built a distribution of power maxima. It appears that, in random data sets, power maxima exceed $p = 0.40$ only once every 100 trials, and never exceed $p = 0.43$ over 10,000 trials. This suggests a False Alarm Probability (FAP) $< 1/10,000$ for the 7.3-d period seen in the original periodogram. Moreover, for a

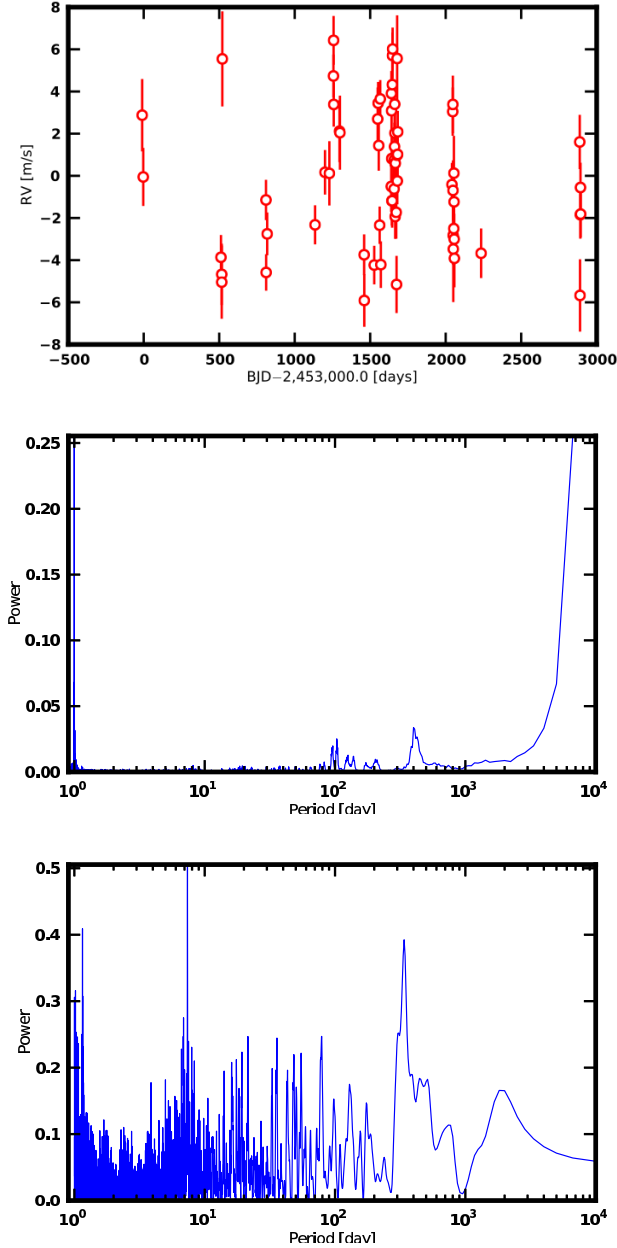


Fig. 2. Top : HARPS radial velocity of Gl 433. Middle : window function of the measurement. Bottom : Periodogram of the HARPS measurements.

more precise estimate of this low FAP value, we made use of Cumming (2004) analytic formula : $FAP = M \cdot (1 - p_{max})^{(N-3)/2}$, where M is the number of independent frequencies in the periodogram, p_{max} its highest power value and N the number of measurements. We approximated M by $2904/1$ (the ratio between the time span of our observations and the typical 1-day sampling), and obtained the very low FAP value of 4×10^{-7} .

We modeled that first periodic signal by a Keplerian orbit. Even though the periodicity was securely identified we used *Yorbit* (an heuristic algorithm, mixing standard non-linear minimisations and genetic algorithms; Ségransan et al. in prep; Bonfils et al. 2011a) and benefited from a global search without *a priori*. We converged on a period $P = 7.3732 \pm 0.0023$ d, semi-amplitude $K_1 = 2.99 \pm 0.38$ m/s and eccentricity $e = 0.17 \pm 0.13$ which, for $M_\star = 0.48 M_\odot$ converts to $m \sin i = 5.49 \pm 0.70 M_\oplus$

(Table 2). The rms and $\sqrt{\chi^2}$ around the solution decreased to 2.17 m/s and 2.00 ± 0.09 per degree of freedom, respectively.

Inspecting the residuals and their periodogram, we measured the power of the most powerful peak ($P \sim 2900$ d; $p_{max} = 0.28$) and apply bootstrap randomization to find it is insignificant ($FAP = 22\%$). We nevertheless found that adding a quadratic drift to the 1-planet model did improve the solution (rms=1.91 m/s and $\sqrt{\chi^2} = 1.79 \pm 0.09$ per degree of freedom).

4.2. HARPS+UVES measurements

Radial velocity measurements of Gl 433 were also obtained with UVES by Zechmeister et al. (2009). They span 2553 days between March 2000 and March 2007 and can therefore extend the time span of our observations by more than 3 years (see Fig. 3 - second panel).

Hence we pooled together UVES and HARPS data and performed again a *1 planet* fit with *Yorbit*. We converged on the same solution with more precise orbital parameters ($P = 7.37131 \pm 0.00096$ d; $K_1 = 2.846 \pm 0.248$ m/s; $e = 0.13 \pm 0.09$). The residuals around the solution show a power excess at a similar period than before ($P \sim 2857$ d; $p_{max} = 0.19$) that now appears more significant. With 10,000 trials of bootstrap randomization we found a $FAP \sim 0.2\%$. Although such signal requires additional measurements for confirmation it justified the addition of a second planet to our model.

With a model composed of 2 planets on Keplerian orbits, *Yorbit* converges on periods of 7.37029 ± 0.00084 and 3690 ± 250 days, with semi-amplitudes of 3.113 ± 0.224 and 3.056 ± 0.433 m/s and eccentricities 0.08277 ± 0.07509 and 0.17007 ± 0.09428 (see. Table 3 for the full set of parameters). The solution has a rms=2.39 m/s and a $\sqrt{\chi^2} = 1.30 \pm 0.05$ per degree of freedom, showing that the combination of HARPS and UVES data sets largely improved the parameter uncertainties.

4.3. The planetary system around Gl 433

In the past, Gl 433 was announced as hosting a brown dwarf of 30 Jupiter mass with an orbital period of ~ 500 days from astrometric measurements Bernstein (1997). But all radial velocity measurements published after, as the present one, reject this detection.

Apparent Doppler shifts may also originate from stellar surface inhomogeneities, such as plages and spots, which can break the balance between light emitted in the red-shifted and the blue-shifted parts of a rotating star (e.g. Saar & Donahue 1997; Queloz et al. 2001; Desort et al. 2007). However the large rotation period (>40 days) of Gl 433 ensures that the observed doppler shift of 7.37 days does not originate from the stellar activity. A search of correlation between the 7.37 days radial velocity period and H_α , CaII-index or bisector is unsuccessful in our HARPS data. Such signal is easily detected when the radial velocity variation is due to activity for a period of ~ 35 days (and *a fortiori* for all shorter periods) (Bonfils et al. 2007; Forveille et al. 2009, see the case of Gl 176 and Gl 674). This is a strong evidence that the ~ 7 d period is not due to stellar surface inhomogeneities but to the presence of a planet orbiting around Gl 433.

This planet, Gl 433b, belongs to the category of super-Earth with a minimum mass of $\sim 5.8 M_\oplus$. At a separation of 0.058AU from its star, Gl 433b is illuminated by a bolometric flux, per surface unity, 10 times higher than what the Earth receives.

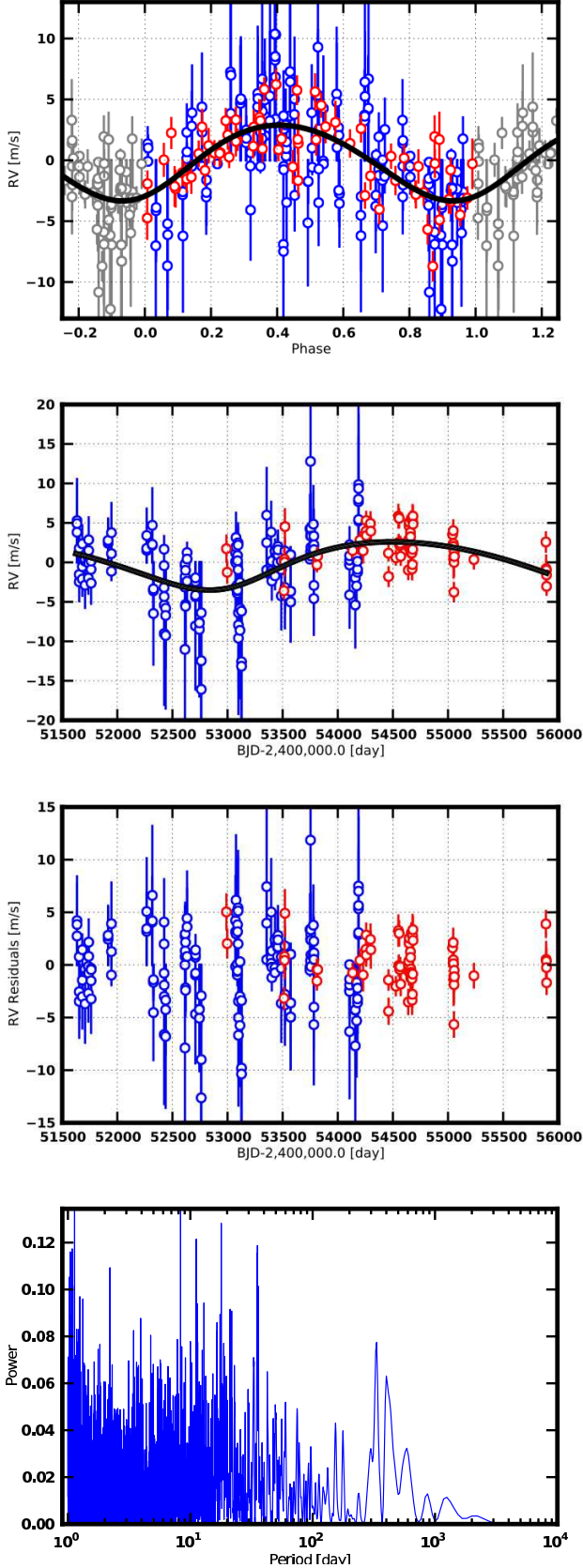


Fig. 3. 2-planets model of HARPS (in red) and UVES (in blue, from Zechmeister et al. 2009) radial velocity measurements for Gl 433. Top : phased radial velocity for a planet of 7.37 days period. Middle : radial velocity curve for the 3700 day period. Below : residuals and their periodogram.

Table 2. Fitted orbital solution for the HARPS data of Gl 433

Gl 433b	
P [days]	7.373 ± 0.002
e	0.17 ± 0.13
T_0 [JD - 2400000]	54597.0 ± 1.0
ω [deg]	136 ± 47
K_1 [m/s]	2.9 ± 0.4
$M_2 \sin i$ [M_{\oplus}]	5.49
a [AU]	0.058
N_{meas}	67
S_{pan} [days]	2904
r.m.s [m/s]	2.17
$\sqrt{\chi^2}$	2.00

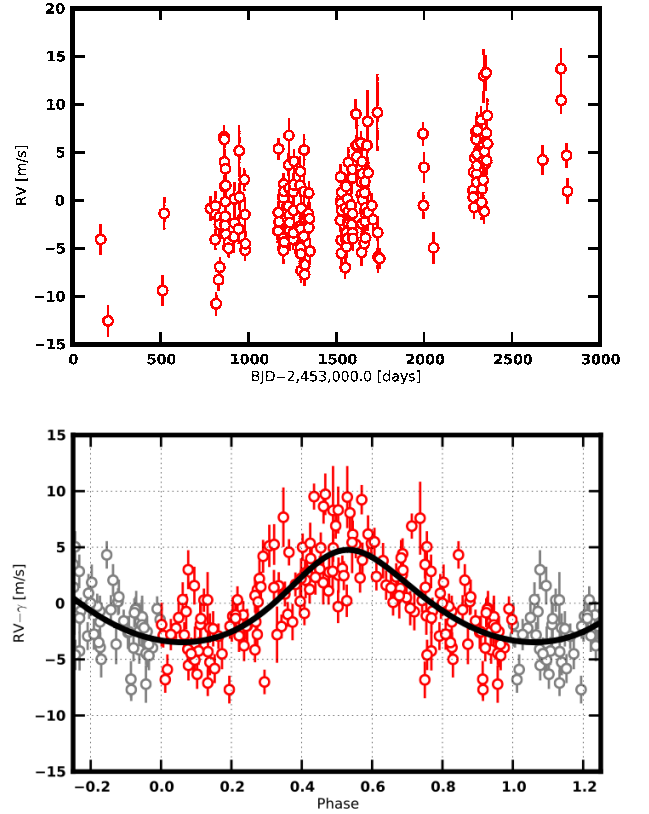


Fig. 4. Top : HARPS radial velocity of Gl 667C. Bottom : one planet plus a linear drift model.

The long period variability detected in the HARPS and UVES data set may have several origins. The signal can have as origin a ~ 10 -year period planet of $50 M_{\oplus}$. A possible origin may also be an effect of a long term stellar magnetic cycle (like the so-called 11-year solar cycle) during which the fraction of the stellar disk covered by plages varies. In such region the magnetic field attenuates the convective flux of the blueshifted plasma and impacts the mean observed radial velocity in the order of few m/s or more (Meunier et al. 2010). Gomes da Silva et al. (2011) do detect large period variation for numerous activity proxy (CaII, NaI, HeI, H_{α} lines) of Gl 433 coherent with a period of ~ 10 years. The RV variability at long period is well correlated with these activity proxies (Gomes da Silva et al. in prep). Therefore, we favor a Magnetic Cycle as the origin of the long term signal.

Table 3. Fitted orbital solution for the HARPS and UVES data of Gl 433

	Gl 433b	Gl 433c
P [days]	7.3709 ± 0.0008	3693 ± 253
e	0.08 ± 0.08	0.17 ± 0.09
T_0 [JD - 2400000]	54287 ± 1	56740 ± 462
ω [deg]	-156 ± 54	-154 ± 36
K_1 [m/s]	3.11 ± 0.23	3.1 ± 0.5
$M_2 \sin i$ [M_\oplus]	5.79	44.6
a [AU]	0.058	3.6
N_{meas}		233
S_{pan} [days]		4259
r.m.s. [m/s]		2.39
$\sqrt{\chi^2}$		1.30

5. Orbital analysis of Gl 667C

We obtained 179 measurements of Gl 667C radial velocity spanning 2657 days between June 2004 and September 2011. The data adds 36 points to those analyzed in Bonfils et al. (2011a) and extend their time span by 1070 days. They have uncertainties of ~ 1.3 m/s (dominated by photon noise) and both rms and $\sqrt{\chi^2}$ values (resp. 4.3 m/s and 3.04 per degree of freedom) indicate a variability above those uncertainties. All RVs are shown as a function of time in Fig. 4 (top panel) whereas their window function and floating-mean periodogram are presented Fig. 5 (top two panels).

5.1. A one planet and linear fit solution

The long-term drift seen in Gl 667C RVs agrees well with the line-of-sight acceleration induced by its companion stellar pair Gl 667AB which is about $GM_{AB}/r_{AB-C}^2 \sim 3$ m/s/yr (for a total mass M_{AB} of $1.27M_\odot$ and a separation of ~ 300 AU). Even without removing that linear drift the periodogram additionally shows a peak at $P \sim 7.2$ days (see Fig. 5, panel b). We do remove an adjusted drift ($\dot{\gamma} = 1.59 \pm 0.14$ m/s/yr) to make the periodic signal even stronger ($p_{max} = 0.53$; Fig. 5 panel c). To measure the FAP of the 7.2 days signal we ran 10,000 bootstrap randomization and found no power stronger than 0.18 suggesting a $FAP \ll 1/10,000$. We also computed the FAP with (Cumming 2004)'s prescription: $FAP = M \cdot (1 - p_{max})^{(N-5)/2}$. We approximate M by $2657/1$ (the ratio between the time span and the typical sampling of our observations) and obtained the extremely low FAP value of $\sim 10^{-25}$. Note that, on Fig. 4 (panel c), a significant and much less powerful peak is seen around $P = 1.0094$ day and corresponds to an alias of the 7.2-day peak with the typical ~ 1 day sampling.

We pursued by adjusting with *Yorbit* the RVs to a model composed of 1 planet plus a linear drift and converged robustly on the orbital elements reported in Table. 5. This model reduced the rms and $\sqrt{\chi^2}$ per degree of freedom to 2.51 m/s and 2.02, respectively. They nevertheless remain above the photon noise and instrumental uncertainties, what prompted us to continue the analysis with the residuals and try more complex models.

5.2. A multi-keplerian plus a linear fit solution

Following up on the periodogram of the residuals around the 1 planet + drift model (Fig 5 panel d), we observed additional power excess around a series of periods, the 6 most powerful peaks being around 28, 91, 105, 122, 185 and 364 d, with $p = 0.225, 0.215, 0.185, 0.181, 0.134$ and 0.123 , respectively.

Table 4. 1 planet + 1 linear drift orbital solution for Gl 667

	Gl 667Cb
P [days]	7.1989 ± 0.0015
e	0.11 ± 0.07
T_0 [JD - 2400000]	54373.4 ± 0.7
ω [deg]	$-22. \pm 36.$
K_1 [m/s]	3.9 ± 0.3
$M_2 \sin i$ [M_\oplus]	5.69
a [AU]	0.0504
γ [km/s]	6.55 ± 0.02
$\dot{\gamma}$ [m/s/yr]	1.26 ± 0.18
r.m.s [m/s]	2.51
$\sqrt{\chi^2}$	2.02

Bootstrap randomization indicates FAPs lower than $1/10,000$ for the 4 most powerful peaks whereas Cumming's prescription attributes them a $FAP < 10^{-12}$.

To model the RVs with 2 planets + 1 drift, one could pick the most powerful peak as a guessed period and perform a local minimization to derive all orbital parameters. We found it is however not the most appropriate approach here because some of the less powerful peaks actually correspond to a signal with high eccentricities, and eventually turned to be better fit. To explore the best solutions we generally prefer the global search implemented in *Yorbit* with eccentricities left to vary freely. We identified several solutions with similar $\sqrt{\chi^2}$ values, reported in Table 5. For all solutions, the first planet and the linear drift keep similar parameter values (see Sect 5.1). On the other hand, the different solutions are discriminated by different orbital periods for the second planet, with P_c equals to $\sim 28, 90, 106, 124, 186$ or 372 days.

To understand those signals we look at the periodograms of the residuals around each solution. We found that, on the one hand, when the solution is with $P_c = 28$ d, the periodogram of the residual shows the remaining peaks at 91, 105, 122, 185 and 364 days (Fig. 6 - panel a). On the other hand, when the solution is with any of the other periods $P_c = 90, 106, 124, 186$ or 372 d then, only the 28 d peak remains (e.g. Fig. 6 - panels b, c, d, e and f). This means that all peaks at 90, 106, 120, 180 and 364 day actually correspond to a single signal, with its harmonics and aliases, and that the peak around 28 d is another independent signal.

One of the 4 signals identified so far (3 periodic signals + 1 linear drift) have ambiguous solutions. Among the possible periods, the ~ 106 -d period seems to correspond to the rotational period of the star as seen in one activity indicator (see. Sect. 5.3). Conservatively, we continue by assuming that signal is due to activity and used the 106-d period to present our fiducial solution. That assumption is given further credit when we run *Yorbit*. Without any *a priori* on any signal, *Yorbit* converges on a solution with $P = 7.2, 28$ and 106 d. We present the orbital parameters of a 3 planet + 1 drift model in Table 6 and the RV decomposition and periodogram of the residuals around that solution in Fig 7. That solution has rms and $\sqrt{\chi^2}$ equal to 1.73 m/s and 1.44 ± 0.06 per degree of freedom, respectively.

Finally, we inspect the residuals around that last model (see panels (e) and (f) in Fig. 7). We found the power maximum of the periodogram located around $P = 1.0083$ d (a possible 1-day alias with a period of 121 day) with power $p_{max} = 0.13$, to which we attributed a FAP of 2.8%. Therefore, we did not consider that significant sine signal remains in the data. Nevertheless, remaining power excess around the period ~ 90 and 122 d suggests the

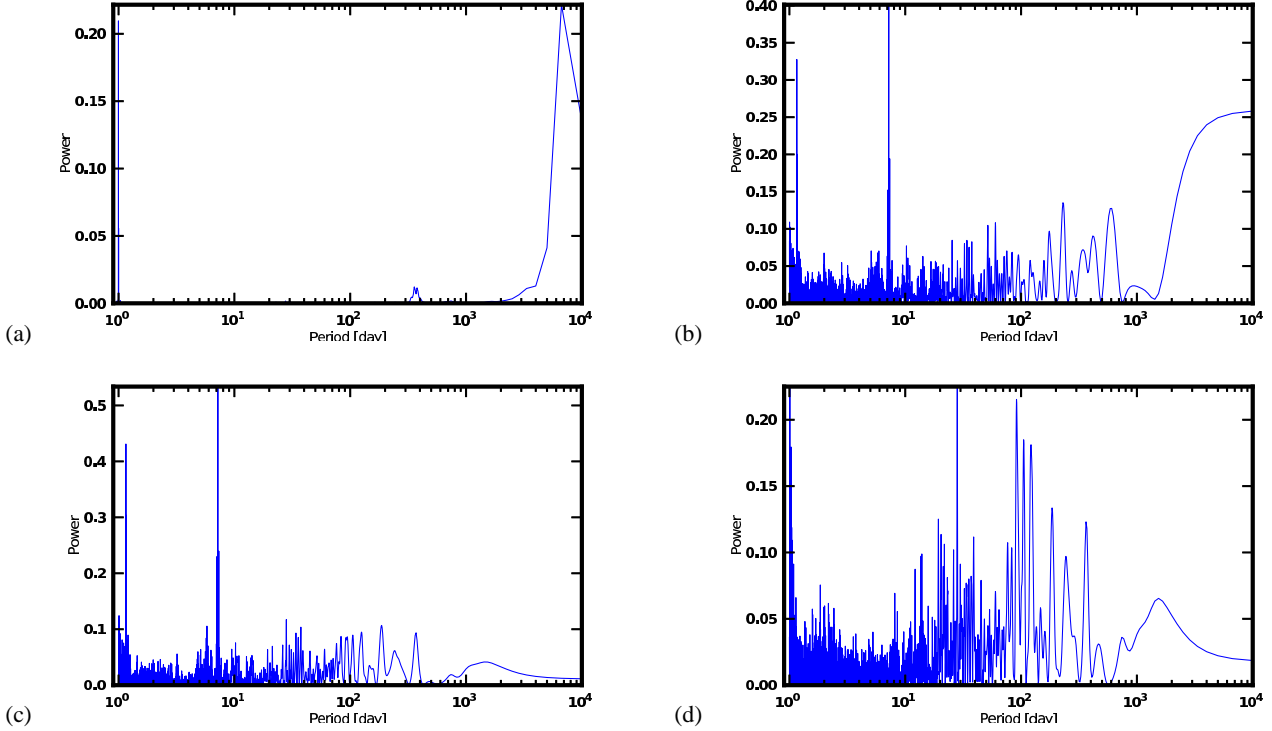


Fig. 5. From the top to the bottom : (a) Window function of the RV measurement; (b) periodograms of the Gl 667C RV measurements; (c) periodograms of the Gl 667C RV measurements after a drift removal; (d) periodograms of the residual after subtraction of a drift + 1 planet model.

Table 6. 3 planets + 1 linear drift orbital solution

	Gl 667Cb	Gl 667Cc	Gl 667Cd
P [days]	7.199 ± 0.001	28.13 ± 0.03	106.4 ± 0.1
e	0.09 ± 0.05	0.34 ± 0.10	0.68 ± 0.06
T_0 [JD - 2400000]	54443.1 ± 0.6	54462 ± 1	54499 ± 1
ω [deg]	-4 ± 33	166 ± 20	7 ± 8
K_1 [m/s]	3.8 ± 0.2	2.0 ± 0.3	2.7 ± 0.4
$M_2 \cdot \sin i$ [M_\oplus]	5.46	4.25	6.93
a [AU]	0.0504	0.1251	0.3035
γ [km/s]	6.55 ± 0.02		
$\dot{\gamma}$ [m/s/yr]	1.85 ± 0.11		
r.m.s. [m/s]	1.73		
$\sqrt{\chi^2}$	1.44 ± 0.06		

keplerian fit does not fully account for the signal we attributed to stellar activity.

5.3. The planetary system around Gl 667C

To assess if one of the radial velocity periodic signal could be due to stellar rotation we searched for periodicity on several activity diagnostics ($H\alpha$ and CaII-index, bisector-inverse slope (BIS) and full-width at half-maximum (FWHM) of the cross-correlation function). The clearest signal detected is a very high peak in the periodogram of the FWHM at a period of ~ 105 days with a FAP lower than 0.1% (see Fig. 8).

Periodic variation of the FWHM is an estimator of the rotation (Queloz et al. 2009). A rotational period of ~ 105 days for Gl 667C is consistent with the faint activity level of these stars, discussed in Sect. 3.2 and such period matches one of the power excess seen in our radial velocity periodogram analysis. Thus

our favorite explanation is that the period of ~ 105 days and all the harmonics or alias at $P = 90, 124, 186$ and 372 days (see Sect. 5.2) are due to stellar rotation. However, we tried to use different sub-sets of RV points and found that the best solution may appear with $P_d = 90, 106$ or 186 d. We therefore consider that the RV signal at large ($P > 90$) period is not definitively assigned to date, its origin may be stellar rotation (the most probable in our point of view), or a high eccentricity planet, 2 planets in resonance or a combination of several of these explanations.

The RV signal at 7.2 and 28.1 d are completely independent of the large period ones and cannot be due to stellar rotation. Thus at least 2 super-Earths are present at close separation of Gl 667C with a mass of 5.5 and 4.25 M_\oplus . Already announced by our team in Bonfils et al. (2011a) with GTO-HARPS data, the use of supplementary HARPS RV allows us to specify their parameters. At a separation of 0.05 and 0.12 a.u. from their star, Gl 667Cb and Gl 667Cc are respectively illuminated by a bolometric flux, per surface unity, 5.51 and 0.89 times than what the Earth receives from the Sun (in using stellar luminosity of Table 1). The super-Earth Gl 667Cc is then in the middle of the habitable zone of its star. We discuss this point in detail in the next section.

6. A planet in the middle of the habitable zone of an M dwarf

6.1. Gl 667Cc

Super-Earths in the habitable zone of their host stars, which by definition is the region where liquid water can be stable on the surface of a rocky planet (Huang 1959; Kasting et al. 1993), currently garner considerable interest. For a detailed discussion of the HZ we refer the reader to Selsis et al. (2007)

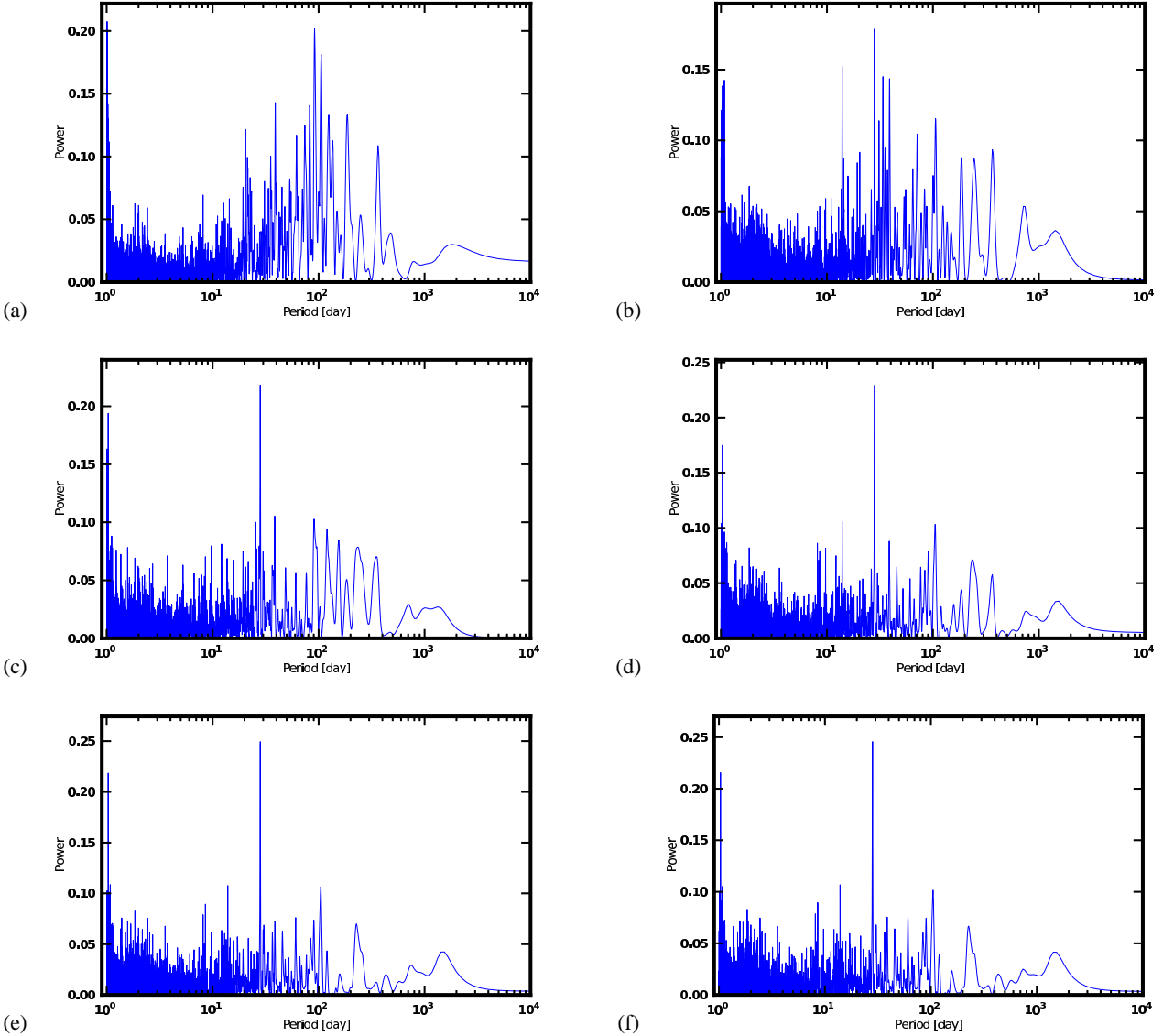


Fig. 6. Periodograms for the Gl 667C residual of radial velocity measurements after subtraction of a drift plus a 2 planet solution. For all the panels the period of the first planet is $P_b = 7.2$ days. From the left to the right and from the top to the bottom the period of the second planet is $P_c = 28, 90, 106, 124, 186$ and 372 days.

or Kaltenegger & Sasselov (2011), but we summarize the most salient points. One important consideration is that a planets with masses outside the $0.5\text{--}10M_\oplus$ range cannot host liquid surface water. Planets under the lower end of this range have too weak a gravity to retain a sufficiently dense atmosphere, and those above the upper end accrete a massive He-H envelope. In either case, the pressure at the surface is incompatible with liquid water. The $10M_\oplus$ upper limit is somewhat fuzzy, since planets in the $3\text{--}10M_\oplus$ range can have very different densities (reflecting different structure) for a given mass: Earth-like, Neptune-like, and Ocean planets can all exist for the same mass (e.g. Fig. 3 in Winn et al. 2011).

To potentially harbor liquid water, a planet with a dense atmosphere like the Earth needs an equilibrium temperature between 175K and 270K (Selsis et al. 2007; Kaltenegger & Sasselov 2011, and references therein). If $T_{eq} > 270\text{K}$, a planet with a water-rich atmosphere will experience a phase of runaway greenhouse effect (see Selsis et al. 2007). At

the other end of the range, CO_2 will irreversibly freeze out from the atmosphere of planets with $T_{eq} < 175\text{K}$, preventing a sufficient greenhouse effect to avoid freezing of all surface water. Either case obviously makes the planet uninhabitable. The inner limit of the habitable zone is well constrained. The outer one, by contrast, is very sensitive to the complex and poorly constrained meteorology of CO_2 clouds, through the balance between their reflecting efficiency (which cools the planet) and their greenhouse effect (which warms it) (Forget & Pierrehumbert 1997; Mischna et al. 2000; Selsis et al. 2007). Finally, a location inside the habitable zone is a necessary condition for hosting surface water, but by no means a sufficient one: long term survival of surface water involves complex ingredients such as a carbonate-silicate geological cycle, and an adequate initial H_2O supply.

Adopting the notations of Kaltenegger et al. (2011) the equilibrium temperature of a planet is:

$$T_{eq} = ((1 - A)L_{star}/(4\beta D^2))^{1/4} \quad (1)$$

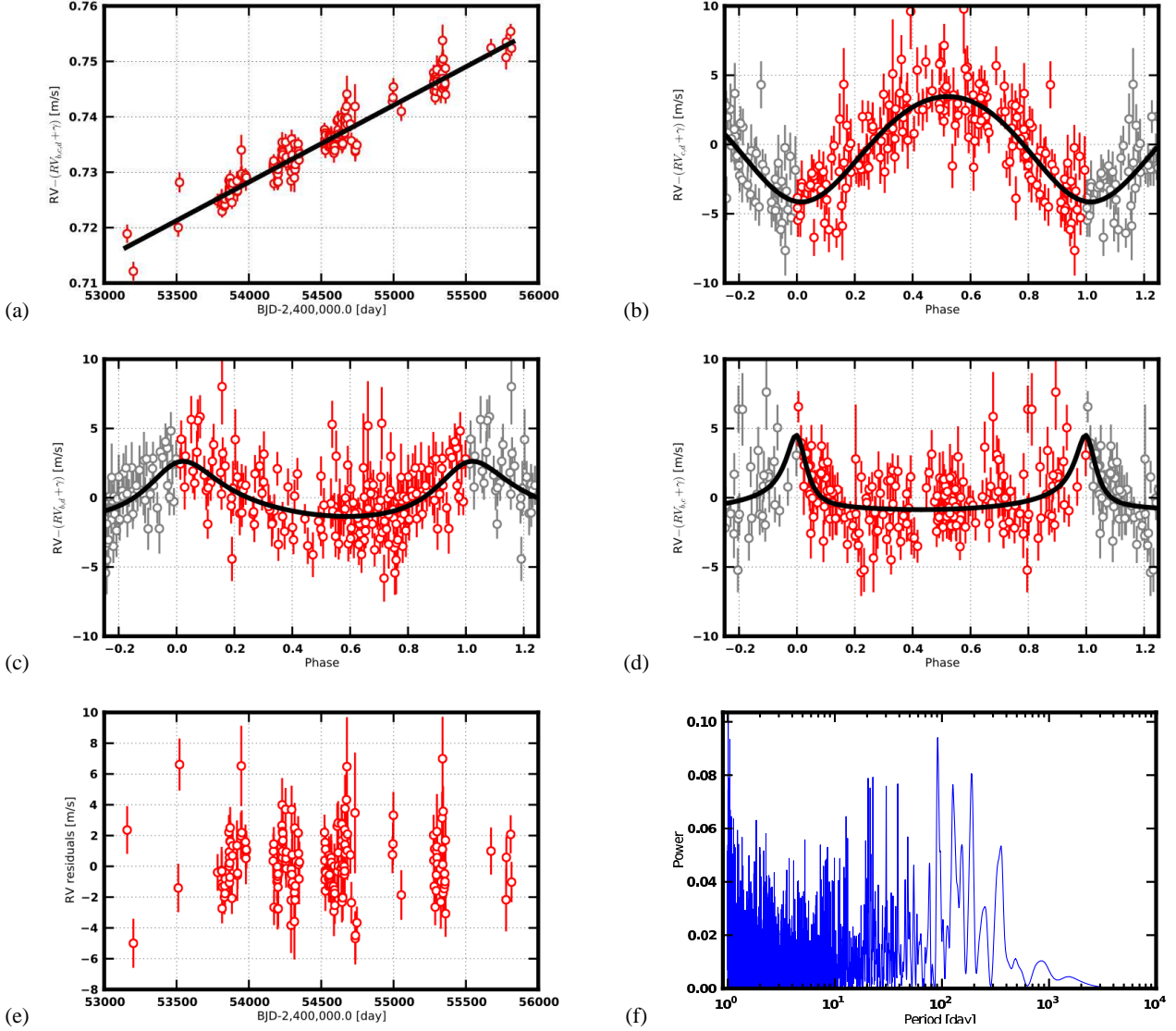


Fig. 7. Decomposition of our nominal 3 planet + 1 drift model for Gl 667C. (a) panel shows the contribution of the long-term drift with the 3 Keplerian contribution removed. Panels b, c and d show respectively radial velocity curves for keplerian $P_b = 7.2$ d, $P_c = 28.1$ d and $P_d = 106.4$ d. Residual of this solution is showed in panel e with their periodogram in panel f.

where β is the geometrical fraction of the planet surface which re-radiates the absorbed flux ($\beta = 1$ for a rapidly rotating planet with a dense atmosphere, like the Earth; $\beta = 0.5$ for an atmosphere-less planet that always presents the same side to its star) and A the wavelength-integrated Bond albedo. Using the stellar parameters of Table 1, the equilibrium temperature of Gl433b and Gl667Cb are respectively $495(\frac{1-A}{\beta})^{1/4}$ K and $426(\frac{1-A}{\beta})^{1/4}$ K. Both planets are firmly in the hot super-Earth category. Gl 667Cc, by contrast, has $T_{eq} = 270(\frac{1-A}{\beta})^{1/4}$ K, to be compared to $T_{eq} = 278(\frac{1-A}{\beta})^{1/4}$ K for the Earth.

Recent 3-D atmospheric models (Heng et al. 2011a,b) suggest that Gl667Cc most likely has β close to 1, even in the case it is tidally locked and always shows the same hemisphere to its star, since they find that a modestly dense Earth-like atmosphere ensures a full re-distribution of the incoming energy. That conclusion, *a fortiori*, also applies for the presumably denser atmosphere of a $4.25M_{\oplus}$ planet (Wordsworth et al. 2011). With

$T_{eq} \sim 270(1-A)^{1/4}$ K, Gl667Cc is therefore in the HZ for any albedo in the [0-0.83] range.

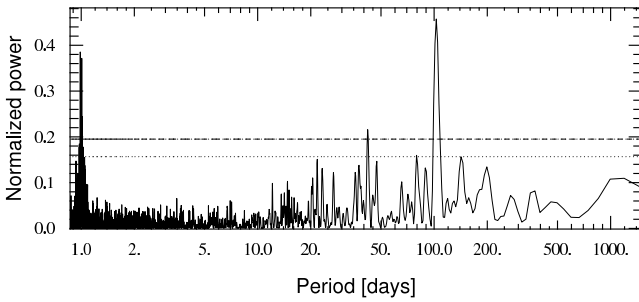
Detailed 3-dimensional atmospheric simulations (e.g. Wordsworth et al. 2011; Heng & Vogt 2011) will need to be tuned to the characteristics of Gl 667Cc to ascertain its possible climate. In the mean time, this planet, which receives from its star 89% of the bolometric solar flux at Earth, is a very strong habitable planet candidate.

6.2. Particularity of the habitable zone around M dwarfs

Two main differences between planets in HZ of solar like stars and M dwarfs are often pointed out. Firstly, a planet in HZ of an M dwarf is closer to its star, and therefore subject to more intense tidal forces. As a result, it is likely to quickly be captured into a spin-orbit resonance. The Solar System demonstrates, however, that this does not necessarily imply that it will be forced into synchronous rotation. The final equilibrium rotation of a tidally influenced planet depends on both its orbital

Table 5. Six commensurable solutions (with similar reduced $\sqrt{\chi^2}$) for the 2-keplerian orbit + 1 drift model

Pl.	P [day]	K [m/s]	T_0 BJD-2, 400, 000.0 [day]	e
b	7.2002±0.0010	4.01±0.26	54443.33±0.53	0.13±0.06
c	28.142±0.031	2.08±0.31	54461.3±1.6	0.32±0.12
	γ	=	6.547 ± 0.020	km/s
	$\dot{\gamma}$	=	1.80 ± 0.13	m/s/yr
	r.m.s.	=	2.15	m/s
	$\sqrt{\chi^2}$	=	1.76 ± 0.05	per degree of freedom
b	7.2002±0.0010	4.19±0.27	54442.89±0.38	0.17±0.06
c	90.24±0.13	2.57±0.61	54483.7±1.3	0.71±0.10
	γ	=	6.548 ± 0.019	km/s
	$\dot{\gamma}$	=	1.75 ± 0.13	m/s/yr
	r.m.s.	=	2.17	m/s
	$\sqrt{\chi^2}$	=	1.77 ± 0.05	per degree of freedom
b	7.2001±0.0010	3.90±0.25	54442.93±0.53	0.13±0.06
c	106.35±0.08	3.30±0.53	54499.46±0.93	0.73±0.06
	γ	=	6.548 ± 0.019	km/s
	$\dot{\gamma}$	=	1.63 ± 0.13	m/s/yr
	r.m.s.	=	2.07	m/s
	$\sqrt{\chi^2}$	=	1.69 ± 0.05	per degree of freedom
b	7.2001±0.0010	3.99±0.27	54442.91±0.45	0.15±0.06
c	123.98±0.14	3.05±0.64	54481.38±0.88	0.80±0.06
	γ	=	6.550 + -0.019	km/s
	$\dot{\gamma}$	=	1.77 + -0.13	m/s/yr
	r.m.s.	=	2.16	m/s
	$\sqrt{\chi^2}$	=	1.71 ± 0.05	per degree of freedom
b	7.2001±0.0010	3.84±0.25	54442.95±0.50	0.14±0.06
c	186.08±0.30	2.79±0.47	54604.4±1.3	0.80±0.05
	γ	=	6.550 ± 0.018	km/s
	$\dot{\gamma}$	=	1.75 ± 0.12	m/s/yr
	r.m.s.	=	2.09	m/s
	$\sqrt{\chi^2}$	=	1.71 ± 0.05	per degree of freedom
b	7.2001±0.0010	3.86±0.25	54442.96±0.49	0.14±0.06
c	372.15±0.57	2.89±0.49	54604.7±1.1	0.87±0.03
	γ	=	6.550 ± 0.018	km/s
	$\dot{\gamma}$	=	1.76 ± 0.12	m/s/yr
	r.m.s.	=	2.09	m/s
	$\sqrt{\chi^2}$	=	1.71 ± 0.05	per degree of freedom


Fig. 8. Periodograms for the FWHM of the correlation peak for the Gl 667C HARPS measurements. A clear peak at ~105 days is well visible and is interpreted as the rotational period of Gl 667C. The line show the 10% and 1% FAP level.

eccentricity and the density of its atmosphere (Doyle et al. 1993; Correia et al. 2008; Correia & Laskar 2010; Heller et al. 2011).

Mercury, for instance, has been captured into the 3:2, rather than 1:1, spin-orbit resonance (Correia & Laskar 2004), and Venus has altogether escaped capture into a resonance because thermal atmospheric tides counteract its interior tides (Correia & Laskar 2003). Whatever the final spin-orbit ratio, the tidal forces will influence the night and day succession, and therefore the climate. As discussed above however, energy redistribution by an atmosphere at least as dense as that of the Earth is efficient (Wordsworth et al. 2011; Heng et al. 2011b,a), and will prevent glaciation and atmospheric collapse on the night side.

The second major difference is stellar magnetic activity, through its dependence on stellar mass. M dwarfs, on average, are much more active than solar-like star. This results from the compounding of two effects: lower mass stars have much longer braking times for stellar rotation (Delfosse et al. 1998; Barnes 2003; Delorme et al. 2011), and for the same rotation period they are more active (Kiraga & Stepien 2007). As a result, a planet in HZ of an early M dwarf receives intense X and UV radiation for 10 times longer than the ~100 Myrs which the solar system spent close to a very active Sun (Ribas et al. 2005; Selsis et al. 2007).

Stellar X and UV radiation, as well as coronal mass ejections (CMEs), could potentially cause a major planetary atmosphere escape (see Scalo et al. 2007; Lammer et al. 2009, for reviews).

Several theoretical studies have looked into the evolution of planetary atmospheres in M-dwarf HZ: do they lose essential chemical species, like H_2O , and can they even be completely eroded out? The problem is complex, with many uncertain parameters, and the span of possible the answers is very wide. Amongst other uncertain factors, the escape ratio sensitively depends on: (1) the intensity and frequency of CMEs for M dwarfs (which is poorly known, and may be much smaller than initially claimed (van den Oord & Doyle 1997; Wood et al. 2005)), (2) the magnetic moment of the planet (a strong magnetosphere will protect the planet against CME-induced Ion Pick Up (Lammer et al. 2007)), and (3) details of the atmospheric chemistry and composition (through atmosphere-flare photochemical interaction (Segura et al. 2010) and IR radiative cooling from vibrational-rotational band (Lammer et al. 2007)). In two limiting cases of planets in M-dwarfs HZ, Lammer et al. (2007) conclude that the atmosphere of an unmagnetized Earth-mass planet can be completely eroded during the Gyr-long active phase of its host star, while Tian (2009) find that the atmosphere of a 7 Earth-mass super-Earth is stable even around very active M dwarfs, especially if that atmosphere mostly contains CO_2 . Continuous outgassing of essential atmospheric species from volcanic activity can, of course, also protect an atmosphere by compensating its escape.

These differences imply that a planet in the habitable zone of an M dwarf is unlikely to be a twin of the Earth. Habitability however is not restricted to Earth twins, and Barnes et al. (2010) conclude that “no known phenomenon completely precludes the habitability of terrestrial planets orbiting cool stars.” A massive telluric planet, like Gl667Cc ($M_2 \cdot \sin i = 4.25 M_\oplus$), most likely has a massive planetary core, and as a consequence a stronger dynamo and a more active volcanism. Both factors help protect against atmospheric escape, and super-Earths may perhaps be better candidates for habitability around M dwarfs than true Earth-mass planets.

6.3. Gl 667Cc compared with the another known planets in the habitable zone

HARPS has previously discovered two planets inside HZ. Gl 581d (Udry et al. 2007; Mayor et al. 2009) ($M_2 \cdot \sin i = 7 M_\oplus$) receives from its M3V host star just $\sim 25\%$ of the energy that the Earth receives from the Sun, and is thus located in the outer habitable zone of its star. Recent detailed models (Wordsworth et al. 2011) confirm that Gl 581d can have surface liquid water for a wide range of plausible atmospheres. HD85512b (Pepe et al. 2011) is a $M_2 \cdot \sin i = 3.5 M_\oplus$ planet in the inner habitable zone of a K5-dwarf, and receives \sim twice as much stellar energy as the Earth. It can harbor surface liquid water if it is covered by at least 50% of highly reflective clouds (Kaltenegger et al. 2011).

Vogt et al. (2010) announced another super-Earth in the HZ of Gl 581, which they found in an analysis combining HARPS and HIRES radial velocity data. The statistical significance of that detection was, however, immediately questioned (e.g. Tuomi 2011), and an extended HARPS dataset now demonstrates that the planet is unlikely to exist with the proposed parameters (Forveille et al. 2011).

Borucki et al. (2011a) announced 6 planetary candidates in the HZ of *Kepler* targets with a radius below twice that of Earth, which they adopt as a nominal limit between telluric and Neptune-like planets. Kaltenegger & Sasselov (2011) reduce

this number to 3 HZ planetary candidates, by discarding 3 planets which they find are too hot to host water if their coverage by reflective clouds is under 50%. Borucki et al. (2011b) recently confirmed Kepler 22b (listed as KOI-87.01 in Borucki et al. (2011a)) as a planet, making it the first planet with a measured radius orbiting in a habitable zone. Kaltenegger & Sasselov (2011) however discarded Kepler 22b from their candidate list because its radius is above 2 Earth-radii.

To summarize, two planets with measured minimum masses in the range for telluric planets (Gl 581d and HD85512b) are known to orbit in habitable zones. Another one, with a measured radius slightly above the nominal limit for a rocky planet, orbits in a similar location (Kepler 22b). Finally, 3 *KEPLER* candidates with radii corresponding to telluric planets and positions in habitable zones currently await confirmation. Gl 667Cc, announced in Bonfils et al. (2011a) and discussed in detail here, is actually the most promising of those for holding conditions compatible with surface liquid water. Receiving $\sim 10\%$ less stellar energy than the Earth and with a minimum mass of $M_2 \cdot \sin i = 4.25 M_\oplus$, it is very likely to be a rocky planet in the middle of the habitable zone of its star.

7. Summary and conclusions

In this paper we analysed in detail 3 super-Earths announced in Bonfils et al. (2011a) : Gl 433b, Gl 667Cb and Gl 667Cc. One, Gl667Cc, is a $M_2 \cdot \sin i = 4.25 M_\oplus$ planet in the middle of the habitable zone of a M1.5V star. It is to date the known extrasolar planet with characteristics closest to Earth, but does not approach being an Earth twin. The main differences from Earth are a significantly higher mass and a different stellar environment, which potentially can have caused divergent evolutions.

Host stars of giant planets are preferentially metal-rich (e.g. Santos et al. 2001, 2004; Fischer & Valenti 2005). The detection rate of planets with masses under $30\text{--}40M_\oplus$, by contrast, does not clearly correlate with stellar metallicity (Mayor et al. 2011). This context makes the discovery of two super-Earths around Gl 667C ($[\text{Fe}/\text{H}] \sim -0.6$, Sect. 3) less surprising, but it remains one of the most metal-poor planetary hosts known to this date, with just 6 planetary host stars listed with a lower metallicity in the Extrasolar Planets Encyclopaedia¹ (Schneider et al. 2011). The metallicity of Gl 433, $[\text{Fe}/\text{H}] \sim -0.2$, is close to the median value of solar neighbourhood, and therefore unremarkable.

Gl 667Cb and c orbit the outer component of a hierarchical triple system. Fewer than 10 other planetary systems, listed in Desidera et al. (2011), share that characteristics. These authors conclude that planets occur with similar frequencies around the isolated component of a triple system and around single stars. The planets around Gl 667C, however, are unusual in orbiting around the lowest-mass component of the system.

The three planets discussed here enter in our Bonfils et al. (2011a) statistical study, which establishes that super-Earths are very common around M dwarfs. Our HARPS survey of ~ 100 stars has, in particular, found two super-Earths in habitable zones, Gl 581d and Gl 667Cc, even though both planets are located in parts of the mass-period diagram where its detection completeness is under 10 percent. This clearly indicates that super-Earths are common in the habitable zones of M dwarfs, with Bonfils et al. (2011a) a $42^{+54}_{-13}\%$ frequency. Future instruments optimized for planet searches around M dwarfs, like the SPIRou (on CFHT) and CARMENES (at Calar Alto observatory) near-IR spectrographs, will vastly increase our inventory

¹ <http://http://exoplanet.eu/index.php>

of such planets around nearby M dwarfs. Such instrument should be able to identify ~50-100 planets in the habitable zones of M-dwarfs, and with a 2-3% transit probability for those, to find at least one transiting habitable planet around a bright M dwarf. Such *radial-velocity educated approach* is already undertaken with HARPS (Bonfils et al. 2011b). In this context we stress that a photometric search for transits must be carried out shortly for Gl 667Cc, which have a 2.5% probability to occur.

Acknowledgements. We thank the 3.6-m team for their support during the observations which produced these results. We thank Abel Méndez for constructive discussion about the “habitability” of Gl 667Cc. Financial support from the “Programme National de Planétologie” (PNP) of CNRS/INSU, France, is gratefully acknowledged. NCS acknowledges the support from the European Research Council/European Community under the FP7 through Starting Grant agreement number 239953, and from Fundação para a Ciência e a Tecnologia (FCT) through program Ciência 2007, funded by FCT (Portugal) and POPH/FSE (EC), and in the form of grants reference PTDC/CTE-AST/098528/2008 and PTDC/CTE-AST/098604/2008. V.N. would also like to acknowledge the support from the FCT in the form of the fellowship SFRH/BD/60688/2009.

References

- Anglada-Escudé, G., Arriagada, P., Vogt, S. S., et al. 2012, ArXiv e-prints
- Barnes, R., Meadows, V. S., Domagal-Goldman, S. D., et al. 2010, ArXiv e-prints
- Barnes, S. A. 2003, ApJ, 586, 464
- Bernstein, H. 1997, in ESA Special Publication, Vol. 402, Hipparcos - Venice '97, ed. R. M. Bonnet, E. Høg, P. L. Bernacca, L. Emiliani, A. Blaauw, C. Turon, J. Kovalevsky, L. Lindegren, H. Hassan, M. Bouffard, B. Strim, D. Heger, M. A. C. Perryman, & L. Woltjer, 705–708
- Bonfils, X., Delfosse, X., Udry, S., et al. 2011a, ArXiv e-prints
- Bonfils, X., Delfosse, X., Udry, S., et al. 2005a, A&A, 442, 635
- Bonfils, X., Forveille, T., Delfosse, X., et al. 2005b, A&A, 443, L15
- Bonfils, X., Gillon, M., Forveille, T., et al. 2011b, A&A, 528, A111
- Bonfils, X., Mayor, M., Delfosse, X., et al. 2007, A&A, 474, 293
- Borucki, W. J., Koch, D. G., Basri, G., et al. 2011a, ApJ, 736, 19
- Borucki, W. J., Koch, D. G., Batalha, N., et al. 2011b, ArXiv e-prints
- Correia, A. C. M. & Laskar, J. 2003, Icarus, 163, 24
- Correia, A. C. M. & Laskar, J. 2004, Nature, 429, 848
- Correia, A. C. M. & Laskar, J. 2010, Tidal Evolution of Exoplanets, ed. Seager, S., 239–266
- Correia, A. C. M., Lestrade, B., & Laskar, J. 2008, A&A, 488, L63
- Cumming, A. 2004, MNRAS, 354, 1165
- Cutri, R. M., Skrutskie, M. F., van Dyk, S., et al. 2003, 2MASS All Sky Catalog of point sources., ed. e. a. Cutri, R. M.
- Delfosse, X., Forveille, T., Perrier, C., & Mayor, M. 1998, A&A, 331, 581
- Delfosse, X., Forveille, T., Ségransan, D., et al. 2000, A&A, 364, 217
- Delorme, P., Collier Cameron, A., Hebb, L., et al. 2011, MNRAS, 413, 2218
- Desidera, S., Carolo, E., Gratton, R., et al. 2011, A&A, 533, A90
- Desort, M., Lagrange, A., Galland, F., Udry, S., & Mayor, M. 2007, A&A, 473, 983
- Doyle, L., McKay, C., Whitmire, D., et al. 1993, in Astronomical Society of the Pacific Conference Series, Vol. 47, Third Decennial US-USSR Conference on SETI, ed. G. S. Shostak, 199
- Fischer, D. A. & Marcy, G. W. 1992, ApJ, 396, 178
- Fischer, D. A. & Valenti, J. 2005, ApJ, 622, 1102
- Forget, F. & Pierrehumbert, R. T. 1997, Science, 278, 1273
- Forveille, T., Bonfils, X., Delfosse, X., et al. 2011, ArXiv e-prints
- Forveille, T., Bonfils, X., Delfosse, X., et al. 2009, A&A, 493, 645
- Gilliland, R. L. & Baliunas, S. L. 1987, ApJ, 314, 766
- Gomes da Silva, J., Santos, N. C., Bonfils, X., et al. 2011, A&A, 534, A30
- Hawley, S. L., Gizis, J. E., & Reid, I. N. 1996, AJ, 112, 2799
- Heller, R., Leconte, J., & Barnes, R. 2011, A&A, 528, A27+
- Heng, K., Frierson, D. M. W., & Phillipps, P. J. 2011a, ArXiv e-prints
- Heng, K., Menou, K., & Phillipps, P. J. 2011b, MNRAS, 413, 2380
- Heng, K. & Vogt, S. S. 2011, MNRAS, 415, 2145
- Huang, S.-S. 1959, PASP, 71, 421
- Kaltenegger, L. & Sasselov, D. 2011, ApJ, 736, L25
- Kaltenegger, L., Udry, S., & Pepe, F. 2011, ArXiv e-prints
- Kasting, J. F., Whitmire, D. P., & Reynolds, R. T. 1993, Icarus, 101, 108
- Kiraga, M. & Stepien, K. 2007, Acta Astronomica, 57, 149
- Kürster, M., Endl, M., Rouesnel, F., et al. 2003, A&A, 403, 1077
- Lammer, H., Bredehöft, J. H., Coustenis, A., et al. 2009, A&A Rev., 17, 181
- Lammer, H., Lichtenegger, H. I. M., Kulikov, Y. N., et al. 2007, Astrobiology, 7, 185
- Leggett, S. K. 1992, ApJS, 82, 351
- Leggett, S. K., Allard, F., Dahn, C., et al. 2000, ApJ, 535, 965
- Louis, C. & Pepe, F. 2007, A&A, 468, 1115
- Mayor, M., Bonfils, X., Forveille, T., et al. 2009, A&A, 507, 487
- Mayor, M., Marmier, M., Lovis, C., et al. 2011, ArXiv e-prints
- Mayor, M., Pepe, F., Queloz, D., et al. 2003, The Messenger, 114, 20
- Meunier, N., Desort, M., & Lagrange, A. 2010, A&A, 512, A39+
- Mischna, M. A., Kasting, J. F., Pavlov, A., & Freedman, R. 2000, Icarus, 145, 546
- Morales, J. C., Ribas, I., & Jordi, C. 2008, A&A, 478, 507
- Muirhead, P. S., Johnson, J. A., Apps, K., et al. 2012, ArXiv e-prints
- Neves, V., Bonfils, X., Santos, N. C., et al. 2012, A&A, 538, A25
- Pepe, F., Lovis, C., Ségransan, D., et al. 2011, A&A, 534, A58
- Pepe, F., Mayor, M., Galland, F., et al. 2002, A&A, 388, 632
- Perrin, M., Cayrel de Strobel, G., & Dennefeld, M. 1988, A&A, 191, 237
- Perryman, M. A. C., Lindegren, L., Kovalevsky, J., et al. 1997, A&A, 323, L49
- Press, W. H., Teukolsky, S. A., Vetterling, W. T., & Flannery, B. P. 1992, Numerical recipes in FORTRAN. The art of scientific computing, ed. W. H. Press, S. A. Teukolsky, W. T. Vetterling, & B. P. Flannery
- Queloz, D., Bouchy, F., Moutou, C., et al. 2009, A&A, 506, 303
- Queloz, D., Henry, G. W., Sivan, J. P., et al. 2001, A&A, 379, 279
- Rauscher, E. & Marcy, G. W. 2006, PASP, 118, 617
- Ribas, I., Guinan, E. F., Güdel, M., & Audard, M. 2005, ApJ, 622, 680
- Saar, S. H. & Donahue, R. A. 1997, ApJ, 485, 319
- Santos, N. C., Israelian, G., & Mayor, M. 2001, A&A, 373, 1019
- Santos, N. C., Israelian, G., & Mayor, M. 2004, A&A, 415, 1153
- Scalo, J., Kaltenegger, L., Segura, A. G., et al. 2007, Astrobiology, 7, 85
- Schlaufman, K. C. & Laughlin, G. 2010, A&A, 519, A105
- Schmitt, J. H. M. M., Fleming, T. A., & Giampapa, M. S. 1995, ApJ, 450, 392
- Schmitt, J. H. M. M. & Liefke, C. 2004, A&A, 417, 651
- Schneider, J., Dedieu, C., Le Sidaner, P., Savalle, R., & Zolotukhin, I. 2011, A&A, 532, A79
- Segura, A., Kasting, J. F., Meadows, V., et al. 2005, Astrobiology, 5, 706
- Segura, A., Walkowicz, L. M., Meadows, V., Kasting, J., & Hawley, S. 2010, Astrobiology, 10, 751
- Selsis, F., Kasting, J. F., Levrard, B., et al. 2007, A&A, 476, 1373
- Söderhjelm, S. 1999, A&A, 341, 121
- Tian, F. 2009, ApJ, 703, 905
- Tuomi, M. 2011, A&A, 528, L5
- Udry, S., Bonfils, X., Delfosse, X., et al. 2007, A&A, 469, L43
- van den Oord, G. H. J. & Doyle, J. G. 1997, A&A, 319, 578
- Vogt, S. S., Butler, R. P., Rivera, E. J., et al. 2010, ApJ, 723, 954
- Winn, J. N., Matthews, J. M., Dawson, R. I., et al. 2011, ApJ, 737, L18+
- Wood, B. E., Müller, H.-R., Zank, G. P., Linsky, J. L., & Redfield, S. 2005, ApJ, 628, L143
- Wordsworth, R. D., Forget, F., Selsis, F., et al. 2011, ApJ, 733, L48+
- Zakhohaj, V. A. & Shaparenko, E. F. 1996, Kinematika i Fizika Nebesnykh Tel, 12, 20
- Zechmeister, M., Kürster, M., & Endl, M. 2009, A&A, 505, 859

Appendix A: Radial velocity measurements

Table A.1. Radial-velocity measurements and errors bars for Gl 433. All values are relative to the solar system barycenter, the secular acceleration is not subtracted (see Sect. 2).

JD-2400000	RV [km.s ⁻¹]	Uncertainty [km.s ⁻¹]
52989.835057	18.167720	0.001660
52996.843978	18.164793	0.001320
53511.574791	18.161194	0.001000
53516.592190	18.160386	0.001400
53516.597028	18.160016	0.001680
53520.601574	18.170608	0.002200
53809.751435	18.164037	0.000900
53810.729535	18.160597	0.000810
53817.770817	18.162430	0.000960
54134.827289	18.162990	0.000870
54200.675734	18.165507	0.001000
54229.642760	18.165469	0.001470
54256.554461	18.170100	0.000960
54257.531401	18.171791	0.001100
54258.495969	18.168751	0.001000
54296.563423	18.167497	0.001410
54299.536021	18.167428	0.001700
54459.849816	18.161704	0.000910
54460.851730	18.159534	0.001190
54526.745535	18.161241	0.000860
54549.673279	18.168181	0.001440
54552.694028	18.168932	0.000950
54556.639741	18.166923	0.001140
54562.685147	18.163146	0.000830
54566.649449	18.169138	0.000840
54570.611066	18.161279	0.001050
54639.547895	18.165018	0.001150
54640.536378	18.169428	0.001010
54641.508220	18.168608	0.000880
54642.531642	18.166339	0.001010
54643.541084	18.164339	0.001120
54645.510158	18.164340	0.001220
54646.510318	18.169850	0.001070
54647.470551	18.171231	0.001030
54648.507247	18.171541	0.000960
54658.462295	18.164905	0.001010
54660.460084	18.166296	0.001280
54661.462908	18.166917	0.001080
54662.473787	18.168927	0.001070
54663.461670	18.167557	0.000860
54664.466903	18.166128	0.001580
54665.470990	18.163598	0.001000
54666.465274	18.166129	0.000900
54672.514921	18.163801	0.001190
54674.470816	18.160382	0.001300
54677.477550	18.166513	0.001150
54678.473044	18.171103	0.001990
54679.476248	18.165294	0.001050
54681.469000	18.166555	0.001200
54682.474358	18.167625	0.000940
55041.491690	18.165273	0.000970
55046.463763	18.168735	0.001090
55047.482719	18.169075	0.001310
55048.480602	18.164995	0.001370
55049.486609	18.162866	0.001340
55050.478302	18.162216	0.002460
55053.476079	18.163187	0.001160
55054.481130	18.165818	0.001710
55055.465316	18.164458	0.001300
55056.458633	18.162689	0.001150
55057.474960	18.161779	0.001320
55234.724210	18.162092	0.001120
55887.861310	18.167640	0.001230
55889.846375	18.160361	0.001660
55891.844384	18.164192	0.001080
55892.857129	18.165482	0.001120
55893.838113	18.164223	0.001060

Table A.2. Radial-velocity measurements and errors bars for Gl 667C (first part). All values are relative to the solar system barycenter, the secular acceleration is not subtracted (see Sect. 2).

JD-2400000	RV [km.s ⁻¹]	Uncertainty [km.s ⁻¹]
53158.764366	6.543610	0.001490
53201.586793	6.535135	0.001530
53511.798846	6.538483	0.001510
53520.781048	6.546518	0.001630
53783.863348	6.547189	0.001130
53810.852282	6.543955	0.001000
53811.891816	6.547456	0.001470
53812.865858	6.546566	0.001200
53814.849083	6.537267	0.000910
53816.857459	6.537278	0.001130
53830.860468	6.539786	0.001060
53832.903068	6.546288	0.001150
53834.884977	6.545569	0.001040
53836.887788	6.541110	0.000910
53861.796371	6.554704	0.001060
53862.772051	6.554435	0.001210
53863.797178	6.552085	0.001020
53864.753954	6.549526	0.001120
53865.785606	6.544717	0.001010
53866.743120	6.545497	0.000930
53867.835652	6.546418	0.001110
53868.813512	6.547938	0.001090
53869.789495	6.551369	0.001130
53870.810097	6.549639	0.001290
53871.815952	6.544530	0.001290
53882.732970	6.543226	0.000960
53886.703550	6.543739	0.000910
53887.773514	6.543099	0.000860
53917.737524	6.544316	0.001570
53919.712544	6.548258	0.001610
53921.615825	6.545739	0.000950
53944.566259	6.545142	0.001460
53947.578821	6.553284	0.002550
53950.601834	6.548475	0.001390
53976.497106	6.550300	0.001070
53979.594316	6.546662	0.001620
53981.555311	6.542953	0.001040
53982.526504	6.543634	0.001170
54167.866839	6.545060	0.001080
54169.864835	6.547001	0.001110
54171.876906	6.553622	0.001050
54173.856452	6.546024	0.001090
54194.847290	6.548596	0.001170
54196.819157	6.544307	0.001270
54197.797125	6.543237	0.001430
54198.803823	6.543058	0.001270
54199.854238	6.548529	0.000960
54200.815699	6.549969	0.001040
54201.918397	6.549210	0.001110
54202.802697	6.543940	0.001140
54227.831743	6.547675	0.001410
54228.805860	6.551985	0.001120
54229.773888	6.555056	0.001680
54230.845843	6.549556	0.001100
54231.801726	6.546737	0.001020
54232.721251	6.545807	0.001780
54233.910349	6.545118	0.001980
54234.790981	6.545979	0.001140
54253.728334	6.549170	0.001330
54254.755898	6.544250	0.000980
54255.709350	6.544921	0.001200
54256.697674	6.547251	0.001320
54257.704446	6.549922	0.001180
54258.698322	6.552382	0.001120
54291.675565	6.542981	0.001740
54292.655662	6.545652	0.001250
54293.708786	6.549893	0.001070

Table A.3. Radial-velocity measurements and errors bars for Gl 667C (first part). All values are relative to the solar system barycenter, the secular acceleration is not subtracted (see Sect. 2).

JD-2400000	RV [km.s ⁻¹]	Uncertainty [km.s ⁻¹]
54295.628628	6.551364	0.001490
54296.670395	6.543394	0.001230
54297.631678	6.542745	0.001020
54298.654206	6.541005	0.001200
54299.678909	6.545336	0.001400
54300.764649	6.547517	0.001120
54314.691809	6.544615	0.002400
54315.637551	6.549255	0.001840
54316.554926	6.553586	0.001570
54319.604048	6.540627	0.001070
54320.616852	6.541618	0.001190
54340.596942	6.546989	0.001030
54342.531820	6.545501	0.001010
54343.530662	6.549111	0.001110
54346.551084	6.546453	0.001590
54349.569500	6.543075	0.001270
54522.886464	6.546384	0.001100
54524.883089	6.550905	0.001190
54525.892144	6.548526	0.001070
54526.871196	6.548147	0.000990
54527.897962	6.544307	0.001140
54528.903672	6.542928	0.001240
54529.869217	6.547428	0.001110
54530.878876	6.549299	0.001000
54550.901932	6.541460	0.001060
54551.868783	6.544421	0.001000
54552.880221	6.547682	0.000960
54554.846366	6.549923	0.001180
54555.870790	6.545093	0.001070
54556.838936	6.544144	0.000980
54557.804592	6.543654	0.001090
54562.905075	6.548637	0.001050
54563.898808	6.546148	0.001000
54564.895759	6.544538	0.001200
54568.891702	6.552451	0.001480
54569.881078	6.547351	0.001270
54570.870766	6.546062	0.001360
54583.933324	6.547979	0.001560
54587.919825	6.545972	0.001550
54588.909632	6.550822	0.001510
54590.901964	6.551713	0.001400
54591.900611	6.547114	0.001430
54592.897751	6.545115	0.001120
54593.919961	6.544525	0.001140
54610.878230	6.557495	0.001430
54611.856581	6.554205	0.001010
54616.841719	6.553078	0.001360
54617.806576	6.554239	0.001740
54618.664475	6.554319	0.002630
54639.867730	6.551852	0.001550
54640.723804	6.554482	0.001150
54641.766933	6.550433	0.001270
54642.676950	6.549163	0.001090
54643.686130	6.543114	0.001250
54644.732044	6.546094	0.001030
54646.639658	6.552565	0.001430
54647.630210	6.551306	0.001210
54648.657090	6.548607	0.001420
54658.650838	6.544032	0.001370
54660.650214	6.547434	0.001520
54661.760056	6.549334	0.001340
54662.664144	6.550485	0.001440
54663.784376	6.546365	0.001280
54664.766558	6.547196	0.002130
54665.774513	6.544636	0.001340
54666.683607	6.547787	0.001290
54674.576462	6.554292	0.001780

Table A.4. Radial-velocity measurements and errors bars for Gl 667C (third part). All values are relative to the solar system barycenter, the secular acceleration is not subtracted (see Sect. 2).

JD-2400000	RV [km.s ⁻¹]	Uncertainty [km.s ⁻¹]
54677.663487	6.556773	0.003150
54679.572671	6.547294	0.001850
54681.573996	6.551406	0.001550
54701.523392	6.548027	0.001160
54708.564794	6.546551	0.001290
54733.487290	6.557735	0.003860
54735.499425	6.545217	0.001630
54736.550865	6.542707	0.001520
54746.485935	6.542513	0.000990
54992.721062	6.555664	0.001140
54995.741739	6.548206	0.001310
54998.708975	6.552168	0.001460
55053.694541	6.543819	0.001550
55276.882590	6.549938	0.001260
55278.827303	6.549239	0.001340
55280.854800	6.551840	0.001360
55283.868014	6.548172	0.001090
55287.860052	6.553284	0.001120
55294.882720	6.555268	0.001060
55295.754277	6.556069	0.001450
55297.805750	6.551650	0.001190
55298.813775	6.550780	0.001150
55299.785905	6.552531	0.002380
55300.876852	6.553712	0.001240
55301.896438	6.556232	0.001730
55323.705436	6.557295	0.001270
55326.717047	6.548716	0.001680
55328.702599	6.550098	0.001470
55335.651717	6.551042	0.001640
55337.704618	6.554643	0.001680
55338.649293	6.561893	0.002660
55339.713716	6.553104	0.001920
55341.789626	6.547775	0.001200
55342.720036	6.554016	0.001580
55349.682257	6.552810	0.001440
55352.601155	6.562211	0.001750
55354.642822	6.555963	0.001140
55355.576777	6.553083	0.001430
55358.754723	6.557765	0.001710
55359.599377	6.554845	0.001450
55673.791183	6.553326	0.001470
55777.715412	6.562886	0.001990
55779.530103	6.559617	0.001290
55809.547632	6.553884	0.001180
55815.538689	6.550158	0.001250